Thermoacoustic Instabilities in Gas Turbines and Rocket Engines: Industry meets Academia
May 30 – June 02, 2016
Munich, Germany
Paper No.: GTRE-014

Two-step approach for pressure oscillations prediction in gas turbine combustion chambers

Dmytro Iurashev[1], Giovanni Campa[2], Vyacheslav V. Anisimov[2], and Ezio Cosatto[2]

Abstract

Currently, gas turbine manufacturers frequently face the problem of strong acoustic combustion driven oscillations inside combustion chambers. These combustion instabilities can cause extensive wear and sometimes even catastrophic damage of combustion hardware. This requires prevention of combustion instabilities, which, in turn, requires reliable and fast predictive tools. We have developed a two-step method to find stability margins for which gas turbines can be operated without going into self-excited pressure oscillations. As first step we perform a set of Unsteady Reynolds-Averaged Navier-Stokes (URANS) simulations with the Flame Speed Closure (FSC) model implemented in OpenFOAM environment to obtain the Flame Transfer Function (FTF) of the combustor setup. As second step we perform time-domain simulations employing low-order network model implemented in Simulink. In this work we apply the proposed method to the BRS test rig developed at the Technische Universität München.

Keywords

Combustion instabilities, industrial gas turbine, time domain simulations

Introduction

Nowadays gas turbine manufacturers have to meet ecological requirements, particularly emissions of NO_X. These requirements force to produce gas turbines that work in lean combustion regime. However, the operation in lean combustion regime is characterized by high probability of combustion instabilities occurrence (see Lieuwen and Yang (2005); Huang and Yang (2009); Sirignano (2015)), which may cause catastrophic damages. This requires prevention of combustion instabilities, which, in turn, requires understanding of the nature of their occurrence.

There are different methods and numerical tools for prediction of combustion instabilities occurrence. The numerical tools used for thermoacoustic analysis could be divided into two groups: those that perform frequency domain analysis (Nicoud et al. (2007); Camporeale et al. (2011); Rofi et al. (2015)) and those that make time domain simulations (Pankiewitz and Sattelmayer (2003); Li and Morgans (2015)). The first type of analysis can be applied to complex geometries of combustion chambers and simulations are relatively fast. One of the main drawback of this type of analysis is that it does not take into account the non-normality of the thermoacoustic problem, as evidenced by Wieczorek et al. (2011). This implies that some modes could experience short-time amplification even though they decay exponentially in the long-time limit. As a result, if the right perturbation is applied to the thermoacoustic system, it could lead to the growth of pressure perturbations in combustion chamber of gas turbine, as reported by Balasubramanian and Sujith (2008).

The second type of tool for the prediction of combustion instabilities occurrence consists in performing simulations in the time domain. In this type of analysis non-normal effects can be taken into account. However, brute force time domain simulations of thermoacoustic processes in gas turbine chambers with complex geometries are extremely expensive from the computational point of view, especially, if there is a need to find the dependence of stability on different parameters of the system and a set of simulations has to be performed. This is the reason why we propose a method in which processes that happen on different scales are modeled in two different tools.

First, we compute the response of the flame to low-amplitude acoustic excitations with the help of Unsteady Reynolds-Averaged Navier-Stokes (URANS) simulations using the Flame Speed Closure (FSC) model implemented in OpenFOAM environment (Iurashev et al. (2015)). As a result, we get the Flame Transfer Function (FTF) of the setup. Second, we use a simplified wave-based approach implemented in Simulink to find a set of parameters under which gas turbines could be operated without going into self-excited pressure oscillations. The obtained FTF is approximated with an appropriate model and is used in the Simulink environment.

Li and Morgans (2015) have shown that simulations in time-domain using wave-based approach with nonlinear flame model can forecast different nonlinear behaviour of thermoacoustic systems. The strong feature of simulations of time domain is that it is possible to predict the unstable frequencies of the system just knowing the FTF. And it is possible to predict amplitude of these oscillations as soon

[1]Università degli studi di Genova, DICCA, Italy
[2]ASEN, Ansaldo Sviluppo Energia S.r.l., Italy

Corresponding author:
Dmytro Iurashev, Università degli studi di Genova, DICCA, Via Montallegro, 1, 16145 Genova, Italy.
Email: dmytro.iurashev@edu.unige.it

as the Flame Describing Function (FDF) - the response of the flame to velocity perturbations of various amplitudes - is found.

In the current work the proposed two-step method is tested on the Beschaufelter RingSpalt (BRS) test rig developed by Komarek and Polifke (2010) at the Technische Universität München. Dependence of stable and unstable frequencies of the setup on several parameters is discussed.

Background

Description of the Flame Speed Closure model

In order to model the combustion in the BRS test rig we use Flame Speed Closure (FSC) model proposed by Lipatnikov and Chomiak (2002). We have implemented this flame model into the *XiFoam* solver of OpenFoam 2.3.0 (2014). This is a solver for simulation of compressible premixed/partially-premixed combustion with turbulence modeling. It uses compressible PIMPLE (merged PISO-SIMPLE) algorithm. The solver makes use of the regress variable, i.e. the normalized fuel mass fraction, defined as

$$b = \frac{T_b - T}{T_b - T_u}, \tag{1}$$

where T_b is the temperature of the burnt gas, T is the temperature of gas at the current point and T_u is the temperature of the unburnt gas. Thus, regress variable is equal to 1 in the zone of unburnt gas and to 0 in the zone of burnt gas.

The FSC model describes the propagation of the flame in the limit case of the absence of turbulence as well as in the case of fully developed turbulence. Moreover, it takes into account the dependence of turbulent diffusivity and turbulent flame speed on the time of flow propagation from the flame holder to the flame front. The transport equation for the regress variable is

$$\frac{\partial \rho b}{\partial t} + \nabla \cdot (\rho \mathbf{U} b) - \nabla \cdot [\rho(\kappa + D_{t,t})\nabla b] = \\ = -\frac{S_{L,0}^2}{4(\kappa + D_{t,t})}\rho_u(1-b)b - \rho_u S_{t,t}|\nabla b|, \tag{2}$$

where ρ is the density of the air-fuel mixture, t is the time, $\mathbf{U}$ is the vector of the mean velocity, κ is the molecular diffusivity, $D_{t,t}$ is the time-dependent coefficient of turbulent diffusion, $S_{L,0}$ is the unperturbed laminar flame speed, $S_{t,t}$ is the time-dependent turbulent flame velocity, The time-dependent coefficient of turbulent diffusion is calculated as

$$D_{t,t} = D_t \left[1 - \exp\left(-\frac{t_{fd}}{\tau'}\right)\right], \tag{3}$$

where D_t is the coefficient of turbulent diffusion, t_{fd} is the flame development time, τ' is the Lagrangian time scale of turbulence, calculated as $\tau' = D_t/u'^2$, where u' is the velocity perturbation. The coefficient of turbulent diffusion is calculated as $D_t = \mu_t/(\rho Sc_t)$, where μ_t is the dynamic viscosity and Sc_t is the turbulent Schmidt number. The flame development time is calculated as follows

$$t_{fd} = \frac{x - x_{fh}}{u_{FSC}}, \tag{4}$$

where x is the current axial position, x_{fh} is the axial position of the flame holder, u_{FSC} is the axial flow velocity at the burner exit. The turbulent flame velocity which depends on the flame development time is calculated as

$$S_{t,t} = S_t \left\{1 + \frac{\tau'}{t_{fd}}\left[\exp\left(-\frac{t_{fd}}{\tau'}\right) - 1\right]\right\}^{0.5}, \tag{5}$$

where S_t is the turbulent flame speed, calculated as

$$S_t = A(u')^{0.75} S_{L,0}^{0.5} \alpha_u^{-0.25} l_t^{0.25}, \tag{6}$$

where A is the model dimensionless constant taken to be equal to 0.52, as recommended by Lipatnikov and Chomiak (2002), α_u is the thermal diffusivity of the unburnt mixture, l_t is the turbulence length scale that is calculated as

$$l_t = C_D \frac{(u')^3}{\epsilon}, \tag{7}$$

where C_D is the model dimensionless constant, ϵ is the turbulence dissipation rate. The heat release rate is proportional to the RHS of Eq. 2, i.e.

$$\dot{Q} \propto \frac{S_{L,0}^2}{4(\kappa + D_{t,t})}\rho_u(1-b)b + \rho_u S_{t,t}|\nabla b|. \tag{8}$$

It is not necessary to know the dimensioned value of the heat release rate, because in further calculations it is normalized by its mean value.

Flame Transfer Function

The dynamic response of a flame to a flow perturbation of small amplitudes can be represented in the frequency domain by its Flame Transfer Function $FTF(\omega)$ (also called frequency response of the flame). It relates fluctuations of mass flow rate or velocity u'_r at a reference position r upstream of the flame to fluctuations of the flame heat release $\dot{Q}'$

$$FTF(\omega) = \frac{\dot{Q}'(\omega)/\bar{\dot{Q}}}{u'_r(\omega)/\bar{u}_r}. \tag{9}$$

Here fluctuations $\dot{Q}'$ and u'_r are normalized against the respective mean values of heat release $\bar{\dot{Q}}$ and velocity $\bar{u}_r$. In experiments the flame transfer function $FTF(\omega)$ is computed from time series of fluctuations u'_r and $\dot{Q}'$ with spectral analysis applying harmonic excitation with a loudspeaker or siren at the inlet.

Wiener-Hopf inversion

Application of the Wiener-Hopf inversion (WHI) to results of unsteady CFD simulations in order to find the FTF of a burner was initially proposed by Polifke et al. (2001). This method reconstructs the Unit Impulse Response (UIR) of the flame to the velocity perturbation and then transforms it into the frequency response using the z-transform:

$$FTF(\omega) = \sum_{k=0}^{L} h_k e^{-i\omega k \Delta t}, \tag{10}$$

where h_k are coefficients of the UIR; to find them, the auto-correlation matrix Γ and the cross-correlation vector $\mathbf{c}$ of the

time series data $(u'_k, \dot{Q}'_k)$ for $k = 0, ..., N$ are calculated as follows:

$$\Gamma_{ij} = \frac{1}{N-L+1} \sum_{k=L}^{N} \frac{u'_{k-i}}{\bar{u}} \frac{u'_{k-j}}{\bar{u}} \text{ for } i, j = 0, ..., L, \quad (11)$$

$$c_i = \frac{1}{N-L+1} \sum_{k=L}^{N} \frac{u'_{k-i}}{\bar{u}} \frac{\dot{Q}'_k}{\bar{\dot{Q}}} \text{ for } i = 0, ..., L, \quad (12)$$

where N is the number of points in vector of the signal time series, L is assumed length of the vector of the UIR, the filter "memory". To find the vector of coefficients of the UIR, the WHI is performed

$$\mathbf{h} = \Gamma^{-1}\mathbf{c}. \quad (13)$$

Wave-based approach for thermoacoustic simulations

The length of the test rig considered in this work is much larger than its dimensions in the other directions. Thus, it is possible to perform a one-dimensional low-order acoustic analysis.

The test rig is divided into a set of sections with constant cross-sectional area. Pressure, velocity, temperature and density are decomposed into the sum of their mean component (denoted by $\bar{}$) and their fluctuating component (denoted by $'$). Mean values of pressure, velocity, temperature, density and thermophysical properties are assumed to be constant along each section and are changing only from section to section.

Perturbations of pressure and velocity could be represented in terms of downstream and upstream propagating acoustic waves (characteristics) (see Fig. 1):

$$p'(x,t) = f\left(t - \frac{x}{\bar{c}_s + \bar{u}}\right) + g\left(t + \frac{x}{\bar{c}_s - \bar{u}}\right) \quad (14)$$

$$u'(x,t) = \frac{1}{\bar{\rho}\bar{c}_s}\left[f\left(t - \frac{x}{\bar{c}_s + \bar{u}}\right) - g\left(t + \frac{x}{\bar{c}_s - \bar{u}}\right)\right] \quad (15)$$

$$\rho'(x,t) = \frac{1}{\bar{c}_s^2}\left[f\left(t - \frac{x}{\bar{c}_s + \bar{u}}\right) + g\left(t + \frac{x}{\bar{c}_s - \bar{u}}\right)\right] \quad (16)$$

where p' is the fluctuating pressure, f and g are downstream and upstream traveling components of acoustic waves respectively, $\bar{c}_s$ is the mean speed of sound, $\bar{u}$ is the mean velocity, u' is the fluctuating velocity, $\bar{\rho}$ is the mean density, ρ' is the fluctuating density.

In order to connect oscillating variables in different sections we need to know the so-called jump conditions. To find the jump conditions between sections with different cross-section area, the system of linearized equations of conservation of mass and energy (Bernoulli) has to be written in terms of f and g as suggested by Dowling and Stow (2005). We can write the system of equations in case of area change in matrix form as follows

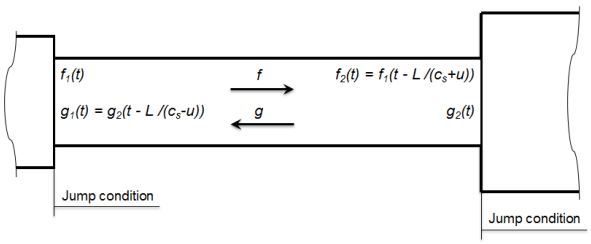

Figure 1. Scheme of waves propagation in a section of a low-order model

$$F\begin{bmatrix} f_d \\ g_u \end{bmatrix} = K\begin{bmatrix} f_u \\ g_d \end{bmatrix}, \quad (17)$$

where subscripts u and d denote upstream and downstream sections respectively. The coefficients of matrices F and K can be found in the Appendix.

To find jump conditions at the flame, the system of linearized equations of conservation of momentum and energy has to be written in terms of f and g. The system of equations in matrix form at the flame is

$$J\begin{bmatrix} f_d \\ g_u \end{bmatrix} = H\begin{bmatrix} f_u \\ g_d \\ \dot{Q}' \end{bmatrix}, \quad (18)$$

where coefficients of matrices J and H can be found in the Appendix.

At the beginning of the first section and at the end of the last section f and g waves are related by the reflection coefficients R_{inlet} and R_{outlet} respectively.

Step 1. Modeling the Flame Transfer Function

Description of the experimental setup

The test rig under consideration is a swirl stabilized atmospheric burner with a central bluff body (see Fig. 2). Methane is burnt in the lean combustion region. Perfectly premixed mixture of methane and air with equivalence ratio equal to 0.77 enters in the setup. The burner exit is represented by an annular section with an inner diameter of 16 mm and an outer diameter of 40 mm. The swirler consists of 8 blades with length of 30 mm is positioned 30 mm upstream the burner exit. Combustion chamber has quadratic cross section of 90×90 mm^2. The length of the combustion chamber is variable and during FTF measurements was kept equal to 300 mm. A perforated plate was placed at the end of the combustion chamber in order to ensure a low reflective acoustic boundary condition. In the experiments the position of the heat release distribution was determined by OH* chemiluminescence measurements. Further details about experimental set-up can be found in the work by Komarek and Polifke (2010).

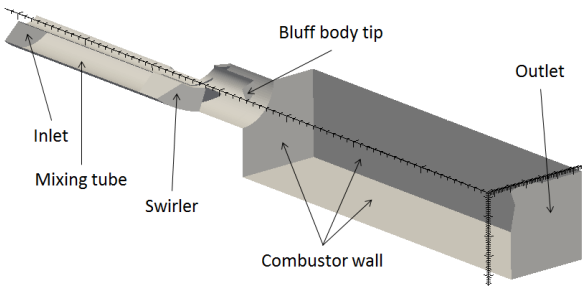

Figure 2. Sector scheme of the numerical set-up of the BRS test rig

Description of the numerical setup

A 3D structured mesh consisting of around 280000 cells was created using the commercial software ANSYS ICEM CFD. Since the structure of the set-up is periodical, just one quarter of the test rig has been modeled in the simulations. For simulations the combustor length of 200 mm was used in the sake of computational costs. It was possible to do so because the heat release zone lays in the first 100 mm of the combustion chamber, as reported by Komarek and Polifke (2010). Thus, the length taken into account was enough to simulate the behavior of the flame. The time step of the simulations is $4 \times 10^{-7} s$ to ensure an acoustic CFL number lower than 0.7.

In investigation the thermal power is equal to 30 kW. To avoid the development of resonance modes, non-reflective or partially reflective boundary conditions at the inlet and at the outlet have been employed. We make use of the *waveTransmissive* boundary condition implemented in OpenFoam 2.3.0 (2014) which is based on the work of Poinsot and Lele (1992) and is expressed as

$$\frac{\partial p}{\partial t} + u_{wave}\frac{\partial p}{\partial x} = \frac{u_{wave}}{l_{inf}}(p_{inf} - p), \qquad (19)$$

where $u_{wave} = u + c_s$ at the outlet, $u_{wave} = u - c_s$ at the inlet, c_s is the speed of sound, l_{inf} is the distance from the boundary (outlet or inlet) at which the pressure field p becomes 0. Boundary conditions for the unperturbed simulation are listed in Table 1.

Table 1. Boundary Conditions for the BRS numerical model

Face	Boundary condition	Details
Inlet	Velocity inlet	11.3 m/s
Outlet	Pressure outlet	101325 Pa
Mixing tube, swirler	Adiabatic no-slip wall	–
Combustor wall	Isothermal no-slip wall	600 K
Bluff body tip	Isothermal no-slip wall	600 K

Results of unperturbed simulations

In a previous work of ours (Iurashev et al. (2015)) a sensitivity analysis of the parameters of the FSC model was described. As a result, the following values of parameters were chosen: the turbulent Schmidt number $Sc_t = 0.3$, the model constant $C_D = 0.3$ and the axial flow velocity at the burner exit $u_{FSC} = 18\ m/s$.

It is illustrative to compare the distributions of heat release in experiments and simulations along the longitudinal axis. To obtain this distribution from our simulation we take several planes perpendicular to the longitudinal axis in the range $0..0.1\ m$ from the beginning of the combustion chamber in the axial direction. Then, we integrate the heat release over these planes and plot the resulting values over the longitudinal axis (see Fig. 3).

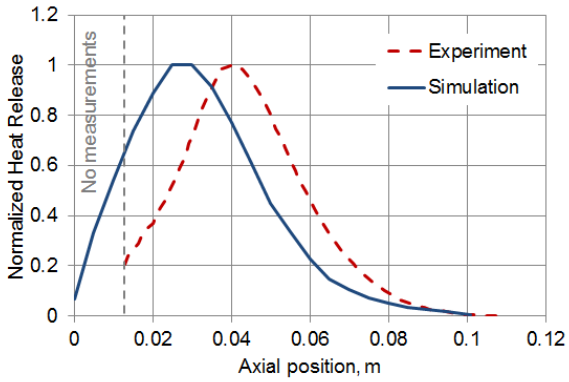

Figure 3. OH* chemiluminescence distribution from experiment and heat release distribution from simulation

The difference between experimental and numerical heat release distributions is explained by the presence of the flame both in the inner and outer shear layers in simulation (so-called M-flame) (Iurashev et al. (2015)). However, in the experiments the flame was observed mostly in the inner shear layer, that is called V-flame. This is explained by the fact that the FSC model was developed for adiabatic cases. Walls of the experimental setup under consideration are made of glass in order to be able to observe the flame and they are not heat-insulated.

FTF numerical calculation

A transient numerical simulation of the system is performed exciting the velocity at the inlet of the computational domain. The signal of excitation is composed of a sum of sines with random frequency in range $0 - 1\ kHz$ and random phase. The excitation signal is normalized in a way that three standard deviations of the signal amplitude are equal to 10% of the mean velocity at the inlet to the computational domain.

The time series u_r is composed during the simulations as the axial component of velocity averaged in the plane perpendicular to the z-axis situated 2 cm upstream of the burner exit (1 cm downstream of the swirler). Response of the flame $\dot{Q}$ is measured in simulations as the volumetric integral of Eq. (8). After that, the mean values $\bar{u}_r$ and $\bar{\dot{Q}}$ of measured u_r and $\dot{Q}$ are computed and are subtracted from series of u_r and $\dot{Q}$ respectively in order to obtain fluctuations of the axial velocity u_r' and fluctuations of the heat release $\dot{Q}'$.

The simulation is run for 129 ms in real time. Longer simulation times do not change the FTF. The duration of the UIR was assumed to be equal to 10 ms. The first 15 ms are considered as transition period and are neglected. Using the Wiener-Hopf inversion method described before, the Flame

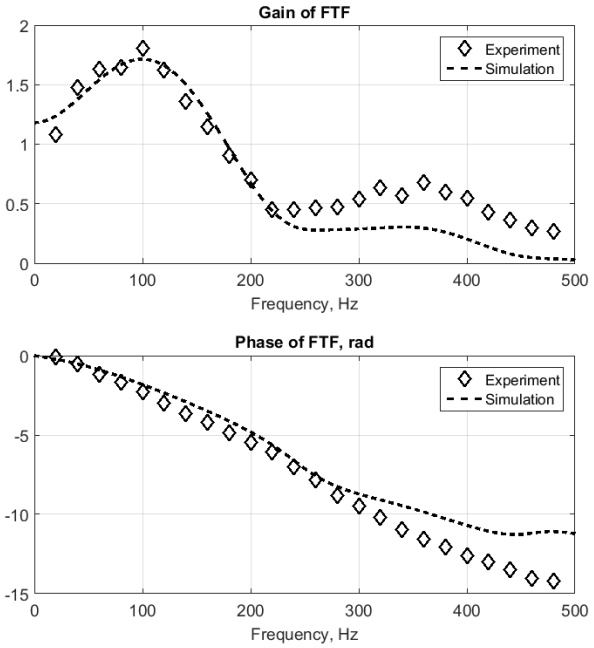

Figure 4. FTF of the BRS test rig obtained experimentally and from simulations in OpenFOAM and Wiener-Hopf inversion

Transfer Function of the BRS test rig is calculated. The results are shown in Fig. 4.

There is a good agreement between the experimentally obtained FTF and the one obtained with simulations in terms of gain of the FTF in range of frequencies from 0 Hz till 300 Hz. The shift in phase of the FTF is explained by the shifted distribution of the heat release from simulations with respect to the experimental one.

Step 2. Stability analysis using wave-based approach

Low-order network model setup

The numerical setup has been divided into 6 regions with 3 jump conditions with pressure losses, one jump condition at the flame and 2 boundary conditions as shown in Fig. 5. The cross-sectional area, length and temperature of each section are listed in Table 2. Jump matrices to connect waves between sections are calculated using systems of Eqs. 17 and 18. The reflection coefficient of the inlet is taken $R_{inlet} = 1$. The outlet reflection coefficient $R_{outlet} = -0.4$ is approximated from the values suggested by Tay-Wo-Chong et al. (2011). The total length of the combustor (sum of the lengths of *Combustor 1* and *Combustor 2*) is $L_{c.c.} = 0.7\ m$ unless other values are specified. Acoustic losses at area changes between plenum and mixing tube and between mixing tube and combustor are taken into account by coefficients of pressure losses $\zeta_{decr} = 0.487$ and $\zeta_{incr} = 0.756$ respectively, calculated by formulae proposed by Idelchik (1992). Acoustic losses at the swirler are taken into account by the coefficient of pressure losses $\zeta_{swirler} = 2.073$ calculated from the unperturbed OpenFOAM simulations. The active flame, i.e. the unsteady heat release, in low-order network model is positioned at $x_{flame} = 0.03\ m$ unless other values are specified. This value corresponds to the maximum of the heat release in the longitudinal direction in OpenFOAM simulations (see Fig. 3).

Table 2. Values of mean flow parameters imposed in the network model

N	Section	Area, m^2	Length, m	Temperature, K
1	Plenum	$3.146E{-}2$	0.17	300
2	Mixing tube 1	$1.056E{-}3$	0.135	300
3	Mixing tube 2	$1.056E{-}3$	0.025	300
4	Mixing tube 3	$1.056E{-}3$	0.02	300
5	Combustor 1	$8.1E{-}3$	x_{flame}	300
6	Combustor 2	$8.1E{-}3$	$L_{c.c.} - x_{flame}$	1930

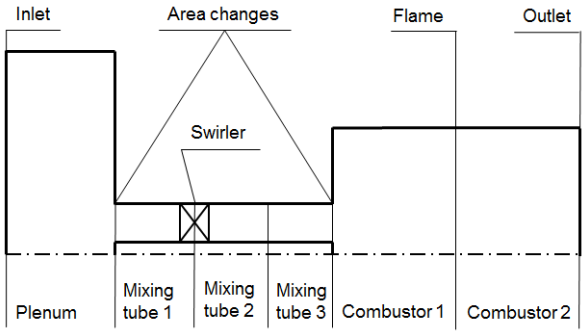

Figure 5. Scheme of numerical setup divided in sections

The setup is excited at the inlet for first $t_{exc} = 0.1\ s$ by the signal composed from sines in the range 0..1 kHz with the maximum amplitude 5 Pa. After 0.1 s till 1.0 s the system is left to evolve by itself without external excitation. We make use of a parameter called cycle increment that gives an information if an acoustic mode is more or less stable. It is possible to calculate the cycle increment from the time domain simulations assuming the following law for the pressure perturbations

$$p'(t) = \sum_{i=1}^{n} P_i sin(2\pi f_i t + \phi_i) e^{\alpha_i (t - t_{exc})} \qquad (20)$$

where f_i is one of the frequencies of pressure oscillations after t_{exc}, n is the number of the frequencies of pressure oscillations after t_{exc}, P_i is the amplitude of pressure oscillations at f_i at the time t_{exc}, ϕ_i is the phase of the pressure oscillations at f_i, α_i is the cycle increment of the mode f_i.

The frequencies of oscillations and their cycle increments are computed by approximating time history of pressure oscillations by Eq. 20 using the least-squares method. In the simulations presented in this work either one or none unstable frequency per run is detected, thus $n = 1$ for all simulations in the network model. Positive values of cycle increment parameter α indicate that the system is unstable, and the negative values of α mean that the system is stable.

FTF approximation for the network model

The FTF obtained from OpenFOAM simulations is inserted in the network model environment in the form

$$FTF_{model}(\omega) = \left[\frac{n_{f,1}\omega_{0,1}^2}{-\omega^2 + 2i\xi_1\omega_{0,1}\omega + \omega_{0,1}^2} + \frac{2in_{f,2}\xi_2\omega_{0,2}\omega}{-\omega^2 + 2i\xi_2\omega_{0,2}\omega + \omega_{0,2}^2} + \frac{2in_{f,3}\xi_3\omega_{0,3}\omega}{-\omega^2 + 2i\xi_3\omega_{0,3}\omega + \omega_{0,3}^2}\right] e^{-i\omega\tau_f} \quad (21)$$

where $n_{f,i}$ is a dimensionless constant, $\omega_{0,1}$ is the cut-off frequency of the second-order low-pass filter, ξ_i is the damping ratio, $\omega_{0,2}$ and $\omega_{0,3}$ are band-pass frequencies, τ_f is the time delay of the flame. Optimum values of coefficients of Eq. 21 are computed using least-squares method and are listed in the Table 3; optimum time delay for the flame model is $\tau_f = 1.163 \cdot 10^{-3}\ s$. The resulting FTF model is shown in Fig. 6 together with the FTF obtained from simulations.

Table 3. Coefficients of the FTF model (Eq. 21)

i	1	2	3
$n_{f,i}$	1.169	1.156	-3.232
$\omega_{0,i}$	2160	1267	1073
ξ_i	0.461	1.612	0.455

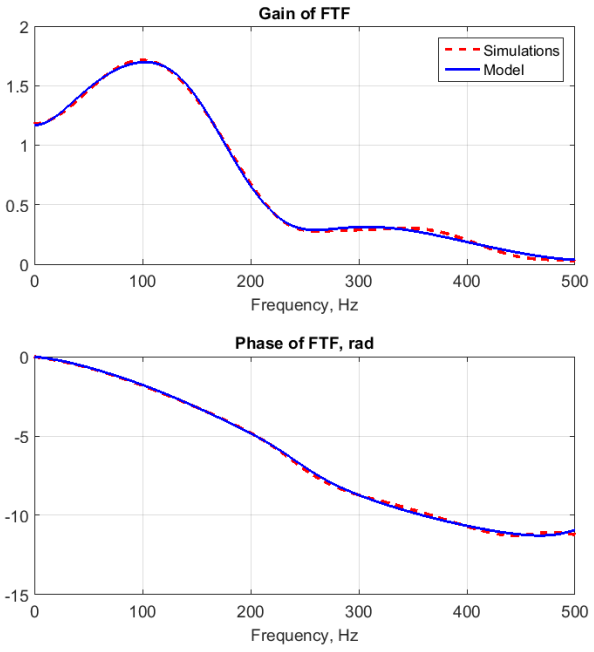

Figure 6. FTF of the BRS test rig from OpenFOAM simulations and modeled with model Eq. 21

Results of network model simulations

An unstable frequency at 101.3 Hz was detected in experiments with a combustor length of 0.7 m as noted by Tay-Wo-Chong et al. (2011). With the length of combustor equal to 0.3 m the setup was stable (Tay-Wo-Chong and Polifke (2012)). We have performed a parametric study with different values of the combustion chamber length in the range 0.3..1.1 m with steps of 0.1 m. For values of the combustion chamber length below and equal to 0.6 m the setup is stable (see Fig. 7). For combustion chamber lengths equal or higher than 0.7 m the setup is unstable. Thus, our simulations predict the setup with the length of combustion chamber $L_{c.c.} = 0.3\ m$ to be stable and with $L_{c.c.} = 0.7\ m$ to be unstable as well as in the experiments. The unstable frequency calculated for $L_{c.c.} = 0.7..1.1\ m$ is around 130..135 Hz and does not depend significantly on the total length of the combustion chamber. The computed frequencies are significantly higher than the one retrieved in experiments. It is worth to mention that this unstable frequency does not correspond to any of the acoustic modes of the setup but is a so-called "flame intrinsic mode", as mentioned by Bomberg et al. (2015).

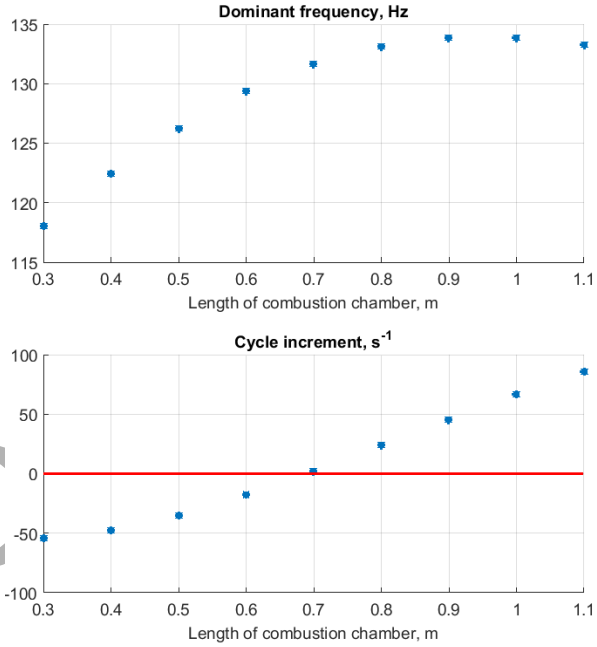

Figure 7. Dominant frequency of oscillations and its cycle increment for various length of combustion chamber; $x_{flame} = 0.03\ m$, $k_G = 1$, $\tau_{add} = 0\ ms$

The FSC model that is used in this work is adiabatic. The Turbulent Flame Closure (TFC) model used by Tay-Wo-Chong et al. (2011) is also adiabatic. However, as noted by Tay-Wo-Chong et al. (2011), using the FTF computed with the URANS simulations with the TFC model predicted the BRS test rig to be unstable only with the total combustor length equal or higher than 1 m. The unstable frequency obtained by Tay-Wo-Chong et al. (2011) is also higher than the one detected in experiments. It is mentioned by Tay-Wo-Chong et al. (2011) that three parameters were different for the experimental measurements and the URANS simulations with the TFC model: the position of the maximum heat release of unperturbed case (denoted here as x_{flame}), the gain and the phase of the FTF around the unstable frequency. To investigate these aspects, we perform a parametric analysis varying the position of the unsteady heat release, the gain and the phase of the FTF in the network model.

Firstly, we calculate the dependence of unstable frequency and its cycle increment on the position of the active flame

with the fixed length of the combustion chamber $L_{c.c} = 0.7\ m$ and the fixed FTF. We vary the parameter x_{flame} in the range $0..0.1\ m$ with steps of $0.01\ m$. This range corresponds to the heat release distribution in the longitudinal direction (see Fig. 3). As it can be seen from Fig. 8 the thermoacoustic system is unstable for values of the x_{flame} smaller or equal to $0.04\ m$. The dependence of α_{dom} on the position of the flame is not as steep as for the dependence of α_{dom} on the length of combustion chamber. When increasing the x_{flame} parameter, the dominant frequency of the setup slightly decreases.

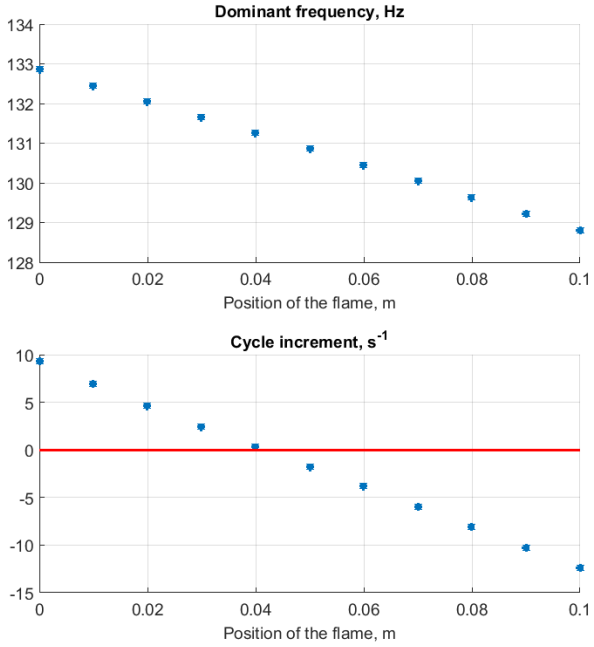

Figure 8. Dominant frequency of oscillations and its cycle increment for various positions of unsteady heat release; $L_{c.c} = 0.7\ m$, $k_G = 1$, $\tau_{add} = 0\ ms$

To study the influence of the gain and the phase of the FTF on the stability of the setup we introduce the modified version of the model for the FTF

$$FTF_{model,2}(\omega) = k_G FTF_{model}(\omega) e^{-i\omega\tau_{add}} \quad (22)$$

where k_G is the dimensionless parameter that is responsible for the change of the gain of the FTF and τ_{add} is the additional time delay that is responsible for the change of the phase of the FTF.

Secondly, we change the parameter k_G in the range $0.8..1.2$ with steps of 0.05. It is seen from the Fig. 9 that the setup is stable for values of k_G lower than 1, i.e. lower values of the gain of the FTF. The dominant frequency of the oscillations of the setup is slowly growing when k_G increases.

Lastly, we vary the parameter τ_{add} in the range $-1.0..2.0\ ms$ with steps $0.2\ ms$. The lower limit of this range is set by the value τ_f. The setup is unstable for higher values of τ_{add}, i.e. higher absolute values of the phase of the FTF, as it can be seen from Fig. 10. The dominant frequency of oscillations decays significantly when τ_{add} is increasing. The unstable frequency $100.3\ Hz$ corresponds to the value

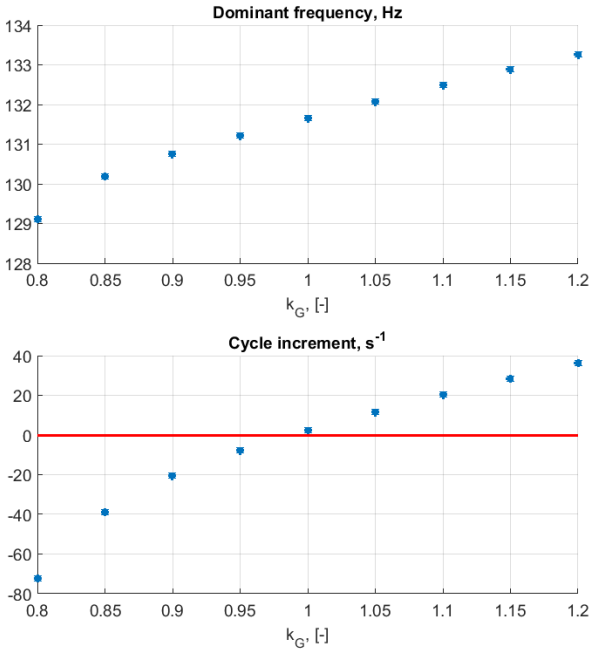

Figure 9. Dominant frequency of oscillations and its cycle increment for various values of k_G parameter; $L_{c.c} = 0.7\ m$, $x_{flame} = 0.03\ m$, $\tau_{add} = 0\ ms$

of the parameter $\tau_{add} = 1.6\ ms$. Almost the same frequency $101.3\ Hz$ was retrived experimentally. It is because the phase of the FTF obtained numerically is underestimated with respect to the experimental one. Adding artificial time delay to the FTF obtained numerically shifts the phase of the FTF closer to the experimental one.

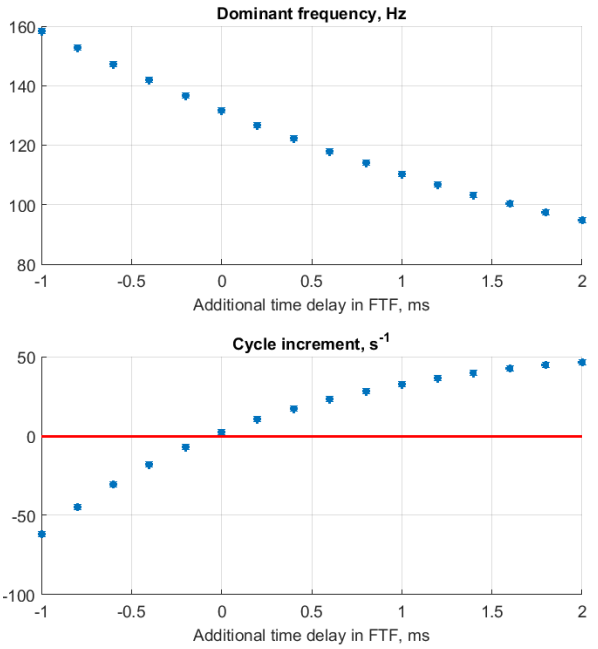

Figure 10. Dominant frequency of oscillations and its cycle increment for various values of τ_{add} parameter; $L_{c.c} = 0.7\ m$, $x_{flame} = 0.03\ m$, $k_G = 1$

Conclusions

In this work we have proposed a two-step analysis of combustion instabilities in time domain. The first step is to obtain the Flame Transfer Function of the system performing URANS simulations with the Flame Speed Closure model implemented in OpenFOAM. The second step is to perform time-domain simulations using wave-based approach implemented in Simulink with the FTF obtained from the first step. We have applied this two-step approach to a laboratory test rig and we have shown that the proposed low-order network model is able to predict combustion instabilities. The unstable frequency computed in simulations corresponds to the unstable frequency detected in experiments. Also the dependence of the stability of the setup on several parameters was investigated successfully.

Acknowledgements

The presented work is part of the Marie Curie Initial Training Network Thermo-acoustic and aero-acoustic nonlinearities in green combustors with orifice structures (TANGO). We gratefully acknowledge the financial support from the European Commission under call FP7-PEOPLE-ITN-2012 during 25/03/2013 24/03/2016. Dmytro Iurashev would like to acknowledge Alp Albayrak for familiarizing himself with the BRS setup and for the consultancy in OpenFOAM environment.

References

Balasubramanian K. and Sujith R.I. (2008) *Non-normality and nonlinearity in combustionacoustic interaction in diffusion flames,* J. Fluid Mech., **594**, 29–57.

Bomberg S., Emmert T., and Polifke W. (2015) *Thermal versus acoustic response of velocity sensitive premixed flames,* Proceedings of the Combustion Institute, **35**, (3), 3185–3192.

Camporeale S.M., Fortunato B., and Campa G. (2011) *A Finite Element Method for Three-Dimensional Analysis of Thermoacoustic Combustion Instability,* J. of Engineering for Gas Turbines and Power, **133** (1), 011506.

Dowling A.P. and Stow S.R. (2005) *Acoustic analysis of gas turbine combustors*. In *Combustion instabilities in gas turbine engines* (e.d Lieuwen T.C. and Yang V.), American Institute of Aeronautics and Astronautics.

Huang Y. and Yang V., (2009) *Dynamics and stability of lean-premixed swirl-stabilized combustion,* Progress in Energy and Combustion Science, **35**, 293–364.

Idelchik I.E. (1992) *Handbook of Hydraulic Resistance, 3rd Edition*, Moscow, Mashinostroienie (in Russian).

Iurashev D., Campa G., Anisimov V., Di Vita A., Cosatto E., Daccà F., and Albayrak A. (2015) *Turbulent Flame Models for Prediction of Pressure Oscillations in Gas Turbine Burners,* Proceedings of the 22^{nd} International Congress on Sound and Vibration, Florence, Italy, 12–16 July 2015.

Komarek T. and Polifke W. (2010) *Impact of Swirl Fluctuations on the Flame Response of a Perfectly Premixed Swirl Burner,* J. Eng. Gas Turbines Power, **132**, p. 061503-1,7.

Li J and Morgans A.S. (2015) *Time domain simulations of nonlinear thermoacoustic behaviour in a simple combustor using a wave-based approach* J. Sound Vib., **346**, 345–360.

Lieuwen, T. C. and Yang, V. (2005) *Acoustic analysis of gas turbine combustors*, American Institute of Aeronautics and Astronautics.

Lipatnikov A.N. and Chomiak J. (2002) *Turbulent flame speed and thickness: phenomenology, evaluation, and application in multi-dimensional simulations,* Progress in Energy and Combustion Science, **28**, 1–74.

Nicoud F., Benoit L., Sensiau C., and Poinsot T. (2007) *Acoustic Modes in Combustors with Complex Impedances and Multidimensional Active Flames,* AIAA Journal **45** (2), 426–441.

OpenFOAM User Guide (2014), Version 2.3.0, 5 February.

Pankiewitz, C. and Sattelmayer, T. (2003) *Time Domain Simulation of Combustion Instabilities in Annular Combustors,* J. of Engineering for Gas Turbines and Power, **123** (3), 677–685.

Poinsot T.J. and Lele S.K. (1992) *Boundary Conditions for direct simulations of compressible viscous flows*, Journal of Computational Physics **101**, 104–129.

Polifke W., Poncet A., Paschereit C. O., and Doebbeling K. (2001) *Reconstruction of acoustic transfer matrices by instationary computational fluid dynamics,* J. Sound Vib. **245**, (3), 483–510.

Rofi L., Campa G., Anisimov V., Daccá F., Bertolotto E., Gottardo E., and Bonzani F., (2015) *Numerical procedure for the investigation of combustion dynamics in industrial gas turbines: LES, RANS and thermoacoustics,* ASME paper GT2015-42168.

Sirignano W.A. (2015) *Driving mechanisms for combustion instability*, London Edinburgh and Dublin Philosophical Magazine and Journal of Science **17**, 419–422.

Tay-Wo-Chong L., Bomberg S., Ulhaq A., Komarek T., and Polifke W. (2011) *Comparative Validation Study on Identification of Premixed Flame Transfer Function,* ASME paper GT2011-46342.

Tay-Wo-Chong L. and Polifke W. (2012) *LES-Based Study of the Influence of Thermal Boundary Condition and Combustor Confinement on Premix Flame Transfer Functions,* ASME paper GT2012-68796.

Wieczorek K., Sensiau C., Polifke W., and Nicoud F. (2011) *Assessing non-normal effects in thermoacoustic systems with mean flow,* Physics of Fluids, **23** (10), 107103.

Appendix A

Matrices for jump conditions between sections for the case of area decrease are

$$F_{decr} = \begin{bmatrix} \frac{S_d}{\bar{c}_{s,d}}(1+M_d) & \frac{S_u}{\bar{c}_{s,u}}(1-M_u) \\ \frac{1}{\bar{\rho}_d}(1+M_d(1+\zeta_{decr})) & -\frac{1}{\bar{\rho}_u}(1-M_u) \end{bmatrix}$$

$$K_{decr} = \begin{bmatrix} \frac{S_u}{\bar{c}_{s,u}}(1+M_u) & \frac{S_d}{\bar{c}_{s,d}}(1-M_d) \\ \frac{1}{\bar{\rho}_u}(1+M_u) & -\frac{1}{\bar{\rho}_d}(1-M_d(1+\zeta_{decr})) \end{bmatrix}$$

where S is the cross-section area, M is the mean Mach number, ζ is the coefficient of pressure losses.

Matrices for jump conditions between sections for the case of area increase are

$$F_{incr} = \begin{bmatrix} \frac{S_d}{\bar{c}_{s,d}}(1+M_d) & \frac{S_u}{\bar{c}_{s,u}}(1-M_u) \\ \frac{1}{\bar{\rho}_d}(1+M_d) & -\frac{1}{\bar{\rho}_u}(1-M_u(1-\zeta_{incr})) \end{bmatrix}$$

$$K_{incr} = \begin{bmatrix} \frac{S_u}{\bar{c}_{s,u}}(1+M_u) & \frac{S_d}{\bar{c}_{s,d}}(1-M_d) \\ \frac{1}{\bar{\rho}_u}(1+M_u(1-\zeta_{incr})) & -\frac{1}{\bar{\rho}_d}(1-M_d) \end{bmatrix}$$

Matrices for jump conditions between sections for the case of temperature jump with active flame and constant cross-section area are

$$J = \begin{bmatrix} (1+2M_d+M_d^2) & -(1-2M_u+M_u^2) \\ \left[\frac{\bar{c}_s+\gamma\bar{u}}{\gamma-1}+\frac{3\bar{u}^2}{2\bar{c}_s}+\frac{\bar{u}^3}{2\bar{c}_s^2}\right]_d & -\left[\frac{\bar{c}_s-\gamma\bar{u}}{\gamma-1}+\frac{3\bar{u}^2}{2\bar{c}_s}-\frac{\bar{u}^3}{2\bar{c}_s^2}\right]_u \end{bmatrix}$$

$$H = \begin{bmatrix} (1+2M_u+M_u^2) & -(1-2M_d+M_d^2) & 0 \\ \left[\frac{\bar{c}_s+\gamma\bar{u}}{\gamma-1}+\frac{3\bar{u}^2}{2\bar{c}_s}+\frac{\bar{u}^3}{2\bar{c}_s^2}\right]_u & -\left[\frac{\bar{c}_s-\gamma\bar{u}}{\gamma-1}+\frac{3\bar{u}^2}{2\bar{c}_s}-\frac{\bar{u}^3}{2\bar{c}_s^2}\right]_d & \frac{1}{S} \end{bmatrix}$$

where γ is the heat capacity ratio.